

Heteroatom-enhanced the Formation of Mesoporous Carbon Microspheres with High Surface Area as Supercapacitor Electrode Materials

Zhuan Gao¹, Xiaobin Huang^{2,*}, Kuiyong, Chen², Chaoying Wan³, Hong Liu²

¹ School of Chemistry and Chemical Engineering, Shanghai Jiao Tong University, Shanghai, China, 200240

² School of Aeronautics and Astronautics, Shanghai Jiao Tong University, Shanghai, China, 200240

³ International Institute for Nanocomposites Manufacturing (IINM), WMG, University of Warwick, UK, CV4 7AL

*E-mail: xbhuang@sjtu.edu.cn

Received: 23 May 2017 / Accepted: 6 September 2017 / Published: 12 October 2017

A novel supercapacitor electrode material based on heteroatom (N, O, P) doped mesoporous carbon microspheres (HMCMSs) was produced via a carbonization of highly cross-linked polyphosphazene microspheres (PMSs), with N, O, P acting as high efficient pore-forming agent. PMSs were synthesized through the polymerization reaction between melamine (MA) and hexachlorocyclotriphosphazene (HCCP). The high level of heteroatom atom of PMSs effectively afforde HMCMSs with high specific surface area (1854.1m²/g), united mesopore structure (pore width ~3nm), as well as high supercapacitor performance. HMCMSs based electrodes exhibited highest specific capacitance of 274 F/g in 6 M KOH aqueous electrolyte at a current density of 0.2 A/g, and excellent cycling durability which had 98.4% capacitance retained even after 2000 cycles. These animative consequences of HMCMSs based electrodes show them great potential in developing high-performance supercapacitors for actual application.

Keywords: Heteroatom-doped; Mesoporous carbon; Polyphosphazene; Supercapacitor

1. INTRODUCTION

Supercapacitors have found broad application prospects involving electric vehicles, uninterruptible power supply and aerospace on account of their desirable characteristics such as excellent electrochemical stability, high power density and safety [1-3]. Nevertheless, the energy density of the current supercapacitor technology still needs to be farther amended without reducing the

cycle stability. As one of the key elements for supercapacitor, the electrode materials are generally derived from carbon materials on account of their large surface area, long circular life, diversity of structure and low cost [4-8]. At the same time, in the actual application for supercapacitors, carbon electrode materials are limited by their low specific capacitance. Porous materials with controllable geometric structure, well-developed aperture structure and high specific surface area can facilitate the formation of electric double layer mechanism of capacitors, and promote the effective transmission of electrolyte ions, so as to provide not only an intensive energy storage capacity but also a corking rate capability [9-11]. Nevertheless, in the present study, the synthesis of porous material combining with high porosity and large specific surface area usually requires additional templates or activating agents, as well as multi-step treatment, which makes the preparation process complex, costly and unfriendly to the environment [12, 13]. Polyphosphazene materials, which have the features of simple preparation, controllable micro/nano-structures, diversity of chemical structures and organic-inorganic hybrid structure, have been reported as ideal precursors of porous carbon material [14, 15]. With the escape of a part of heteroatoms from polyphosphazene at high carbonization temperature, porous carbon with high surface area and porosity can be obtained easily. Additionally, a part of heteroatom doped in the carbon materials can not only fortify the surface wettability of the materials but also induce the pseudocapacitive behavior, which could effectually enhance the specific capacities of carbon materials [16, 17].

In this article, we introduce a facile and extensible method to synthesize a novel type of highly cross-linked polyphosphazene microspheres (PMSs) via one-step polymerization between melamine (MA) and hexachlorocyclotriphosphazene (HCCP). HMCMSs with large BET surface area were facilely obtained via direct carbonization PMSs in a nitrogen atmosphere. Due to the highly cross-linked characters in the structure of PMSs, it is feasible to maintain the geometric structure of PMSs in the carbonization process. Additionally, for the high level of heteroatoms (P, N, O) of PMSs, large BET surface area and uniform mesoporous structure could be formed simultaneously. The unique structure of the HMCMSs is helpful to improve the electronic performance of the electrodes. This work provides an effective strategy to mesoporous carbon materials via carbonization polyphosphazene nano materials with high level of heteroatoms, and used them as high performance supercapacitor electrode materials.

2. EXPERIMENTAL

2.1. Materials

Hexachlorocyclotriphosphazene (HCCP) was bought from Aladdin Industrial Corporation. Melamine (MA), acetonitrile (ACN), triethylamine (TEA) and ethanol were acquired from Sinopharm Chemical Reagent Co., Ltd (Shanghai, China) and used directly. Polytetrafluoroethylene (PTFE) dispersion (60 wt% solid content suspended in water) was received from Aladdin Industrial Corporation. Carbon black (acetylene, 99.9+%, 50% compressed, 75m²/g) was bought from Alfa Aesar (China) Chemical Co. Ltd.

2.2. Synthesis of PMSs

The PMSs were synthesized via fusculation reaction between MA and HCCP in the existence of TEA, which acted as an acid-acceptor. The solvothermal process is summarized as follows: 2.61 g of TEA (25.92 mmol) was added to the solution mixed with HCCP (1.50 g, 4.32 mmol) and MA (1.09 g, 8.62 mmol) in ACN (120 mL). After a deoxidization process, the polycondensation was conducted in a 150 ml PTFE autoclave under 150 °C for 8 h. After the reaction, products were obtained by decentering and washing with alcohol for three times. After being dried under vacuum at 80 °C, PMSs as faint yellow powder were obtained (1.54 g, yield 93%, calculated from HCCP).

2.3. Preparation of HMCMSs

1.50 g of PMSs was thermal-treated in a tube-furnace to obtain HMCMSs. First, the furnace was persistent overheated to 500 °C with a rate of 5 °C /min and equilibrated at 500 °C for 2 h, then the furnace was heated to the target value (750, 800, 850 °C) with a rate of 5 °C /min and equilibrated at target temperature for 2 h in a flow of nitrogen. After the temperature of the furnace decrease to room temperature, we gained the final products. The product was named as HMCMSs-T, where T on behalf of the target carbonization temperature (750, 800 or 850°C).

2.4. Characterization

The micro morphology of the samples was obtained on a NOVA NANOSEM 230 low vacuum field emission scanning electron microscopy (LV UHR FE-SEM) and a TALOS F200X field emission transmission electron microscopy (FE-TEM). The chemical structure of as-prepared PMSs was characterized by a Nicolet 6700 fourier transform infrared spectrometer (FT-IR). Raman spectrums were obtained by using a Senterra R200-L dispersive Raman Microscope with the excitation wavelength at 532 nm. X-ray photoelectron spectroscopy (XPS) patterns were implemented using an AXIS Ultra DLD spectrometer with Al/K α X-ray radiation ($h\nu=1486.6\text{eV}$) and C1s line at 284.8eV as calibration criterion. The X-ray diffraction (XRD) spectrums were performed at a D8 ADVANCE Da Vinci poly-functional X-Ray diffractometer with Cu/K α radiation, where the test pattern was 2θ range from 10 to 70° with a scan rate of 6°/min. The pore structures of the specimens were performed by N₂ physical adsorption at 77 K (ASAP 2010 M+C) after vacuum drying at 200°C. Specific surface areas were obtained by Brunauer–Emmett–Teller (BET) method and a slit/cylindrical nonlocal density functional theory (NLDFT) model was used to count the pore size distribution and pore volume.

2.5. Electrochemical Characterization

To prepare the working electrodes, 80 wt% active material (HMCMSs-T), 10 wt% acetylene black dispersed in ethanol solution and 10 wt% PTFE preparation were mixed to gain a slurry. Subsequently, the slurry was coated onto a nickel foam substrates (1 cm ×1 cm) and pressed at 10MPa

for 20 s then through vacuum drying at 120 °C for 12 h to obtain the final HMCMSs electrodes. Electrochemical performances for HMCMSs supercapacitor were investigated used a three electrode systems in 6 mol L⁻¹ KOH aqueous electrolyte. Cyclic voltammetry (CV), galvanostatic charge/discharge and electrochemical impedance spectroscopy (EIS) measurements were carried out on a CHI660D electrochemical workstation within a potential window of -0.1 to -0.9 V, where Hg/HgO electrode, a Pt-flake (6 cm²) and the prepared electrodes were used as reference, counter and working electrodes, respectively.

Specific capacitance obtained from galvanostatic charge–discharge can be computed accorded to the formula below:

$$C_g = \frac{I\Delta t}{m\Delta V}$$

where C_g (F g⁻¹) represent the gravimetric capacitance; ΔV (V) is the voltage window; m (g) is the mass of active materials; I (A) and Δt (s) stand for the discharging current and time, respectively.

3. RESULTS AND DISCUSSION

HMCMSs were prepared according to the process described in Fig. 1(a). Firstly, PMSs were polymerized between MA and HCCP in the existence of TEA. In the process of reaction, TEA was used as an acid-acceptor to absorb hydrochloric acid (HCl), which was produced from MA reacting with HCCP. The nucleophilic displacement reaction between the P–Cl bonds and amino group was voluntarily expedited with the reaction between TEA and HCCP [9]. The resultant PMSs is about 800 nm in diameter (see in Fig.1(c) and (d)).

FTIR spectrogram of the PMSs was shown in Fig. 2, the characteristic absorption at 3350 cm⁻¹ (a) and 1652 cm⁻¹ (c) represent the stretching vibration of N-H and C-N bond in the structure of MA respectively. The peaks appeared at 1551cm⁻¹ (b) and 815 cm⁻¹ (d) represent the characteristic absorption of the s-triazine in the structure of MA. The absorption at 1209 cm⁻¹ (e) and 962 cm⁻¹ (f) stand for the characteristic absorption of N=P and P–N in the structure of cyclotriphosphazene. Furthermore, the characteristic peaks of the P–Cl band in HCCP at 519 cm⁻¹, 602 cm⁻¹ (g') disappeared after the polycondensation and the peaks at 874 cm⁻¹ (f') of P-N in HCCP blue-shifts to 962 cm⁻¹ (f). The characteristics above indicate that the new P–NH–(s-triazine) band was formed in the structure of PMSs, similar to the results as reported previously [9, 14, 15]. These indicate that the polycondensation reaction between MA and HCCP were successfully achieved as demonstrated in Fig. 1(a).

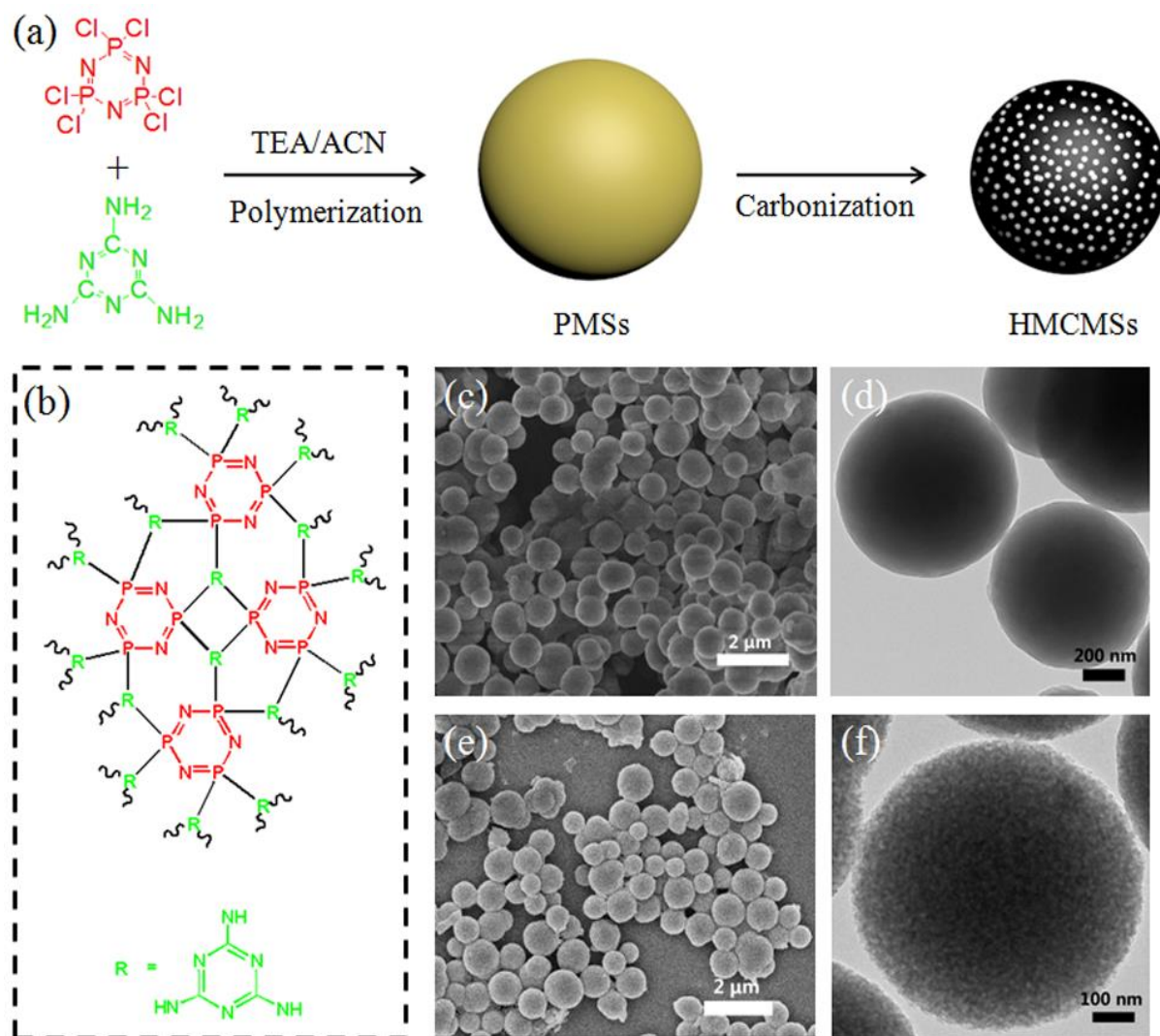


Figure 1. (a) Scheme of HMCMSs preparation; (b) Chemical structure of PMSs; FESEM images of PMSs (c) and HMCMSs-800 (e); FETEM images of PMSs (d) and HMCMSs-800 (f).

Next, PMSs were carbonized under inert atmospheres to achieve HMCMSs, with heteroatoms (N, O, P) acting as high efficient pore-forming agent. The end samples were named as HMCMSs-T and T stands for the target carbonization temperature (750, 800 or 850°C). Fig. 1(e) and (f) show the FESEM and FETEM pictures of HMCMSs-800 respectively. After carbonized, the samples remained the original spherical structure with diameter of about 700 nm and contain abundant pore structure. The key factor to maintain the geometry of the spheres after carbonization is the greatly cross-linked molecular structure (see in Fig. 1(b)) of PMSs, because it could effectively restrain the polymers from melting into large agglomerations in the process of high temperature calcinations [14, 18].

Fig. 3(a) shows the XRD patterns of HMCMSs-T carbonized at various temperatures (750, 800 and 850 °C), the broad diffraction peaks spanning from 27 to 30° indicates a highly disordered and low extent of graphitization structure of the carbon materials [19]. As illustrated in the Raman spectra in Fig. 3(b), the D-band appeared at 1340 cm^{-1} corresponds to the flaws, swing bonds and flexural sheets in the carbon structure, whereas the G-band at 1585 cm^{-1} is usually contribute to the E_{2g} mode of

carbon [20]. Generally, the materials with higher specific value of D-band and G-band (ID/IG) show a lower degree of graphitization. The ID/IG values of HMCMSs-750, HMCMSs-800 and HMCMSs-850 are 0.99, 1.01 and 1.03 respectively, indicating an inferior regularity of the products carbonized at higher temperatures. The results above may be on account of the cracks of in-plane C=C at high carbonization temperature.

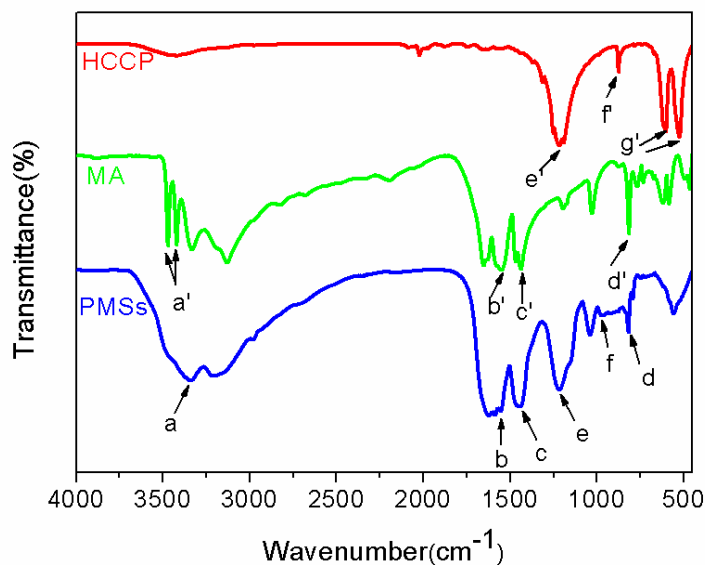


Figure 2. FT-IR spectrums of MA, HCCP and PMSs microsphere

Fig. 3(c) shows the nitrogen adsorption–desorption isotherms of the HMCMSs with different carbonization temperatures. HMCMSs-800 and HMCMSs-850 samples exhibit type-IV isothermals, which correspond to the mesoporous structure in the samples [21]. As is shown in Fig. 3(d), the pore structures of HMCMSs are mainly mesopores with narrow average pore size distribution at ~3 nm. Pore volumes and BET specific surface of the three samples are summarized in Table 1. It should be noted that the large pore volume and high BET surface area of HMCMSs-800 and HMCMSs-850 are obtained without the additional treatment of activator such as CO₂ or KOH [13, 22-23], which shows obvious advantages over other reported processes for activated carbons. Among all samples, HMCMSs-750 exhibited the lowest porosity and lowest BET surface. It is mostly on account of the low calcination temperature, which cause the heteroatoms escaping from the structure of PMSs insufficiently and thus decreasing the formation of high porosity and specific surface area. On account of the high level of heteroatoms in the structure of PMSs, HMCMSs with large BET surface area and uniform mesoporous structure could be obtained easily at high carbonization temperature [14]. At the side of micropores, uniform mesopores are more in favor of the diffusion and transport of electrolyte ions, thus decreasing the ion-transport resistance [24]. These characteristics of HMCMSs would help the electrodes to realize the high power performance at high current densities [25].

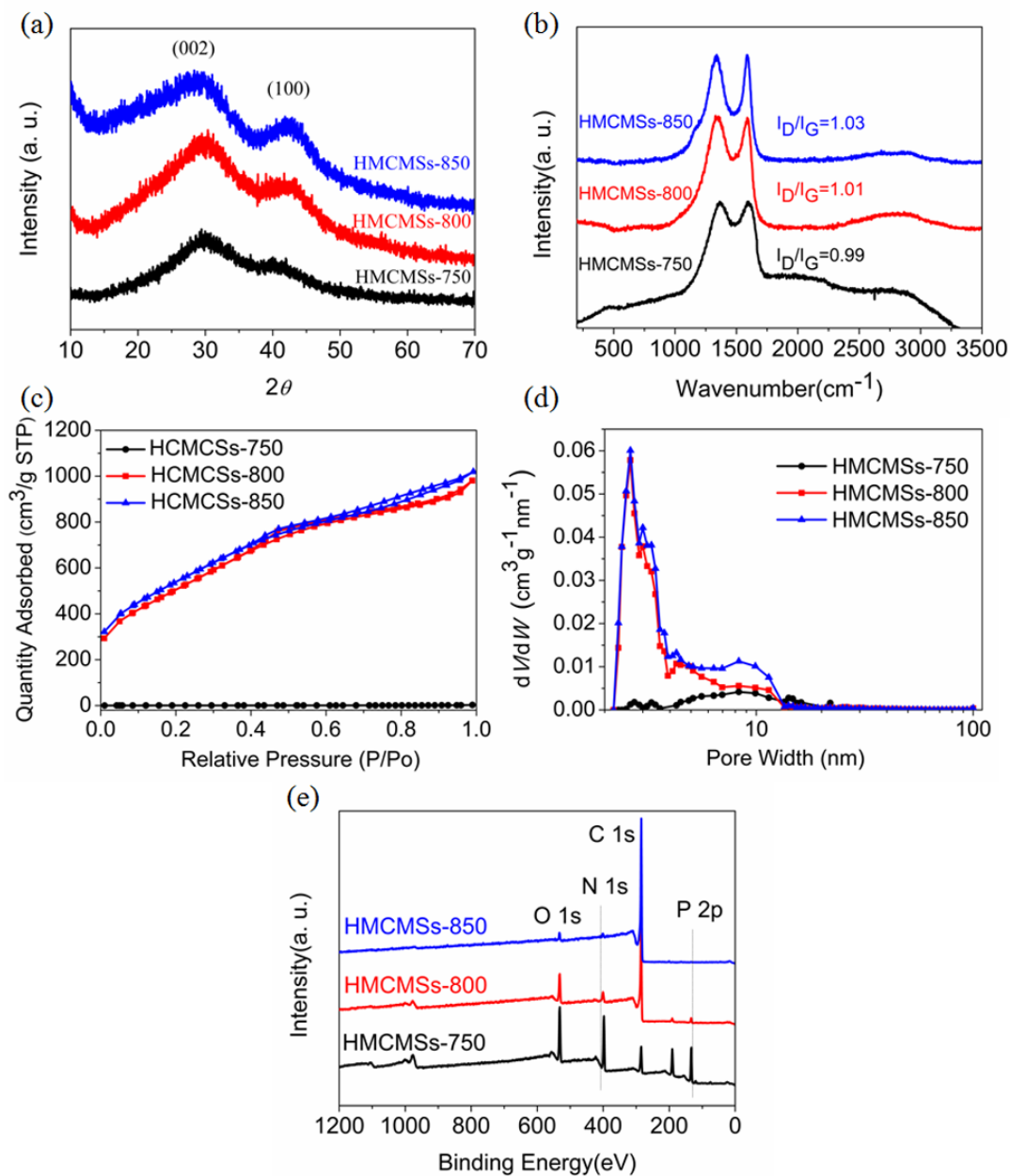


Figure 3. (a) XRD patterns of HMCMSs; (b) Raman spectrums of HMCMSs; (c) N₂ adsorption and desorption isotherms of HMCMSs; (d) Pore size distribution plots of HMCMSs; (e) XPS spectrums of HMCMSs

Fig. 3(e) reveals the XPS spectra of the HMCMSs. C, O, N, and P elements were discovered in the structure of the three samples. The heteroatoms, which mainly stem from the molecular structure of the PMSs, are generally reduced in quantity along with the rise on carbonization temperature (see in Table 1). It is worth noting that the content of heteroatoms could maintain 18.31 at% even after calcined at 800 °C. Heteroatoms (N, P, O) existed in carbon materials have been proved to be beneficial to the specific capacitance [17, 26–27].

Table 1. Constituent elements, BET surface areas and pore volumes of HMCMSs obtained at various temperatures

Sample	C (at.%)	N (at.%)	O (at.%)	P (at.%)	S_{BET}^2 m ² /g	V_{pore}^3 cm ³ /g
HMCMSs-750	35.58	27.62	20.04	16.76	1.8	0.0004
HMCMSs-800	81.69	6.53	9.63	2.15	1854.1	0.7015
HMCMSs-850	94.90	2.15	2.70	0.24	1956.7	0.7595

Cyclic voltammograms of HMCMSs electrodes recorded with a scan rate of 2mV/s in 6 M KOH was presented in Fig. 4(a). The shapes of voltammograms feature distinct rectangular, reflecting the ideal EDLC behavior of HMCMSs electrodes [28]. Among the three samples, HMCMSs-850 exhibited more inerratic rectangle in the face of high scan rates, which was probably profit by the high specific surface area and porosity that bring faster transfer of the electrolyte ions [29]. CV splines of the three samples obtained at different scan rates are demonstrated in Fig. 5. Among the three samples, humps could be observed in the curves of HMCMSs-750 and HMCMSs-800 within a voltage window of -0.4 to -0.7 V. This may be due to the pseudocapacitance effects caused by the high level of heteroatom atom comprised in the surface structures of the active materials.

Similarly, galvanostatic charge-discharge measurements of HMCMSs electrodes were also recorded in 6 M KOH within a voltage window of -0.9 to -0.1 V. Fig. 4(b) illustrates the galvanostatic charge-discharge splines of HMCMSs electrodes when the ampere density was 0.2 A/g. All splines feature near symmetrical triangle patterns, indicating the ideal EDLC behavior of the HMCMSs electrodes. Specific capacitance (C_g) calculated from galvanostatic charge-discharge and area specific capacitances (C_{sa}) versus BET surface area of HMCMSs based electrodes are summarized in Table 2. The C_g of HMCMSs-800 could come up to 274 F/g without activated, much higher than those of other porous carbon that described in the literatures, which was benefit from the high BET surface and united mesoporous structure [14, 30]. HMCMSs-750 shows the lowest gravimetric capacitance because of its extremely low BET surface, whereas, by the reason of large amount heteroatom, which brings the pseudocapacitance, HMCMSs-750 exhibits a very high area specific capacitance. The BET surface of HMCMSs aggrandized rapidly along with the raise of target carbonized temperature, however, the content of heteroatom decreased, which results in a low pseudocapacitance effect, thus the HMCMSs-850 electrode exhibits a relatively lower specific capacitance than the HMCMSs-800. It is noteworthy that the maximal specific capacitance of HMCMSs based supercapacitor could reach 274 F/g without activated when the ampere density was 0.2 A/g, which is vergleichbar to those of activated carbons (ACs), carbon aerogels, carbon nanotube (CNT) and some other carbon materials as supercapacitors (see in Table 3).

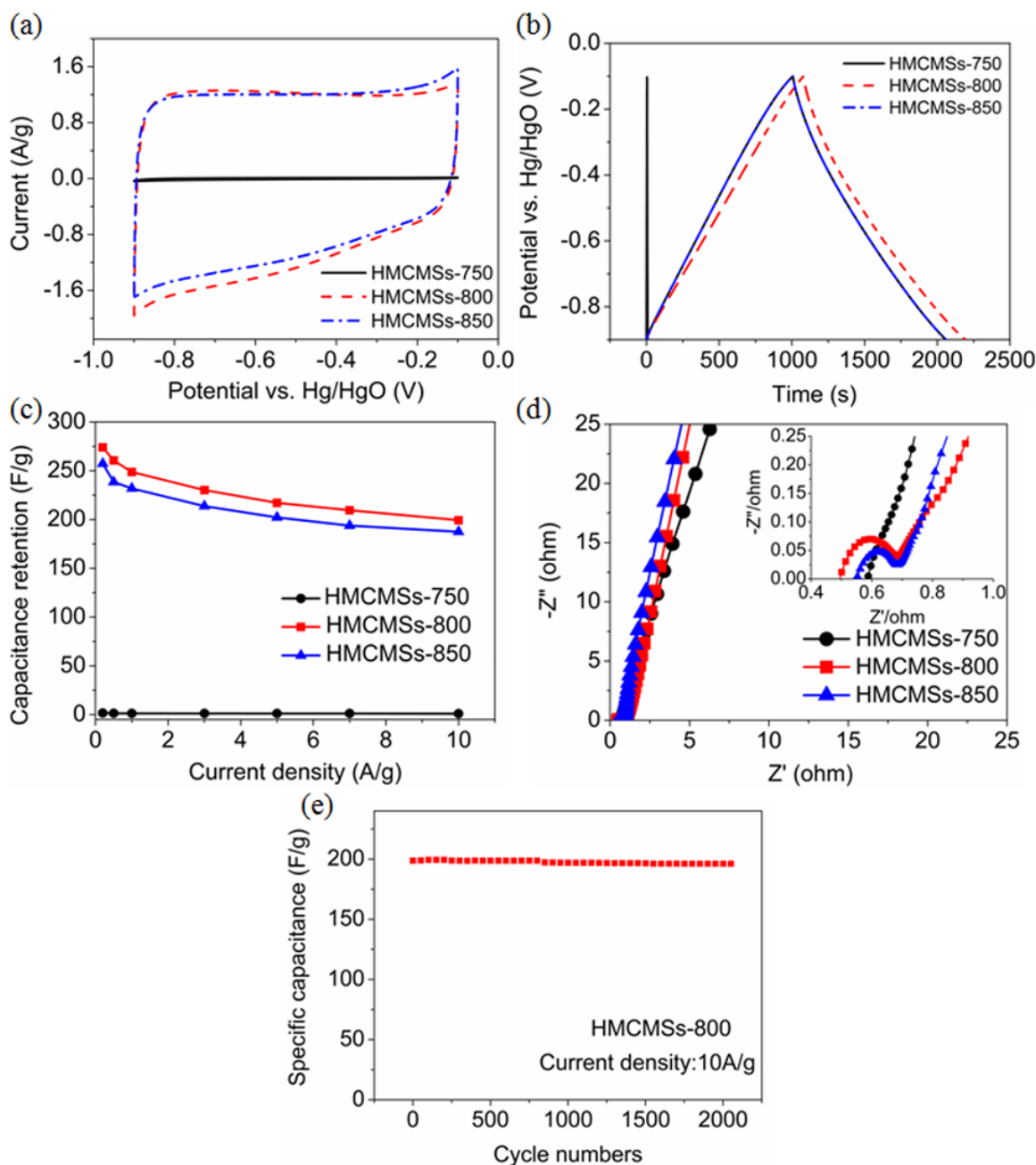


Figure 4. (a) Cyclic voltammograms of HMCMSs electrodes with scan rate of 2 mV/s. (b) Galvanostatic charge-discharge splines of HMCMSs electrodes when the ampere density was 0.2 A/g. (c) Specific capacitances versus ampere density of HMCMSs electrodes. (d) Nyquist plots of HMCMSs (the insert of (d) is an enlarged view of high frequency region). (e) Cyclic life of HMCMSs-800.

Fig. 6 illuminates the galvanostatic charge–discharge splines of HMCMSs recorded at different ampere densities. Fig. 4(c) describes the gravimetric capacitances (C_g) of HMCMSs changed with current densities, where C_g was calculated from galvanostatic charge-discharge. The capacitance retention ($=C_g$ (high current density)/ C_g (low current density) $\times 100\%$) of HMCMSs-750, HMCMSs-800 and HMCMSs-850 could reach 75.4%, 80.2%, and 80.9% respectively when the ampere density

increase from 1 to 10 A/g. Generally, the samples carbonized at higher temperatures exhibits better capacitive preservation under large ampere densities, which are greatly attributed to the large content of mesoporous structures and high BET surface area acquired at high carbonization temperatures. The large content of mesoporous structures could effectually reduce the diffusion resistance of the electrolyte ions.

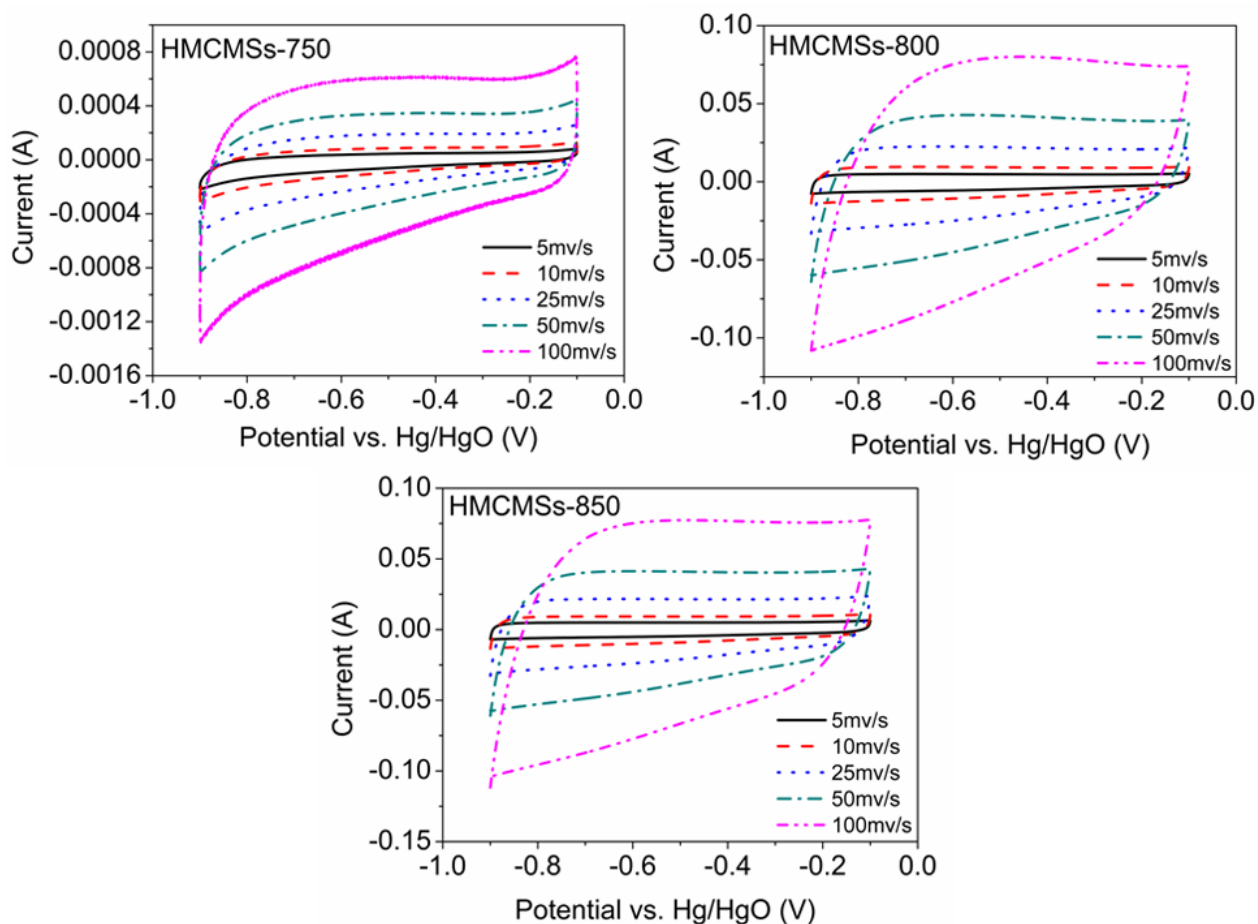


Figure 5. CV splines of HMCMSs at various scan rates

Table 2. Capacitive performance of HMCMSs

Capacitance	HMCMSs-750	HMCMSs-800	HMCMSs-850
C_g^a (F/g)	1.6	274.0	257.4
C_{sa}^b (F/m ²)	0.91	0.15	0.13

^a Gravimetric capacitance when the discharge ampere density was 0.2 A/g.

^b Area specific capacitance obtained through dividing gravimetric capacitance versus by BET surface area.

Table 3. Specific surface area and capacitive performance of various carbon materials for supercapacitors

Carbon materials	BET surface area /m ² g ⁻¹	Specific capacitance /F g ⁻¹
Activated carbons (ACs)	1000–3500	< 200
Templated porous carbons (TC)	1000–3000	120–350
Carbon nanotube (CNT)	120–500	50–100
Carbon fibers (CF)	500–2500	100–300
Carbon aerogels	400–1000	100–125
Graphene	<2360	100–300
Carbon cloth	2500	100–200

To understand the fundamental impedance properties of HMCMSs-based electrodes, electrochemical impedance spectroscopy (EIS) was gauged within a frequency range of 0.1 Hz to 100 kHz under an open circuit potential (see in Fig. 4(d)). In the very high frequency regions, the intercept at real axis (Z') is corresponded to the comprehensive resistance (R_e) combined with ionic resistance of bulk electrolyte, contact resistance of the HMCMSs/Ni foam interface, and intrinsic resistance of HMCMSs [31]. R_e of HMCMSs-750, HMCMSs-800 and HMCMSs-850 are 0.59, 0.49 and 0.55 V respectively, which shows the low electrolyte ions transmission resistance between working and reference electrodes. The diameter of the semicircle in high-frequency range mirrors the proportions of charge-transfer resistance (R_{ct}) ascribed to the double-layer capacitance and Faradic reactions on the active material grain surface. R_{ct} of HMCMSs-800 and HMCMSs-850 are very low about 0.2 and 0.13 V respectively. The straight slop in low frequencies corresponds to the ion transport and diffusion resistance to the electrode surface. As shown in Fig.6d, the straight slop of HMCMSs-850 in the low-frequency range is the largest. It may be a consequence of its large BET surface area and well-developed mesoporous structure that are more conducive to ion transport.

Long cycling life is the critical factor to verdict the performance of supercapacitors. The cycling life measurement of HMCMSs-800 over 2000 cycles in 6 M KOH was conducted by circulating the charge–discharge experiments for 2000 cycles at a ampere density of 10 A/g. Fig. 4(e) exhibits the capacitive retention ratio of HMCMSs electrodes along with the change of the cycle number. As elucidated in Fig. 4(e), the specific capacity of HMCMS-800 nearly remains constant, degenerated only 1.6% compare to the initial specific capacity even after 2000 cycles. Consequently, the capacitive retention of 98.4% for HMCMSs based supercapacitor is vergleichbar to those carbon based supercapacitors, such as hollow carbon microspheres (98.2% reservation after 2000 cycles), carbon fiber (97% reservation over 2000 cycles), grapheme/CNT/CO(OH)₂ (70% reservation after 1500 cycles), grapheme/polypyrrole (96% reservation over 1000 cycles) and active carbons (92% reservation after 2000 cycles) [9,32-35].

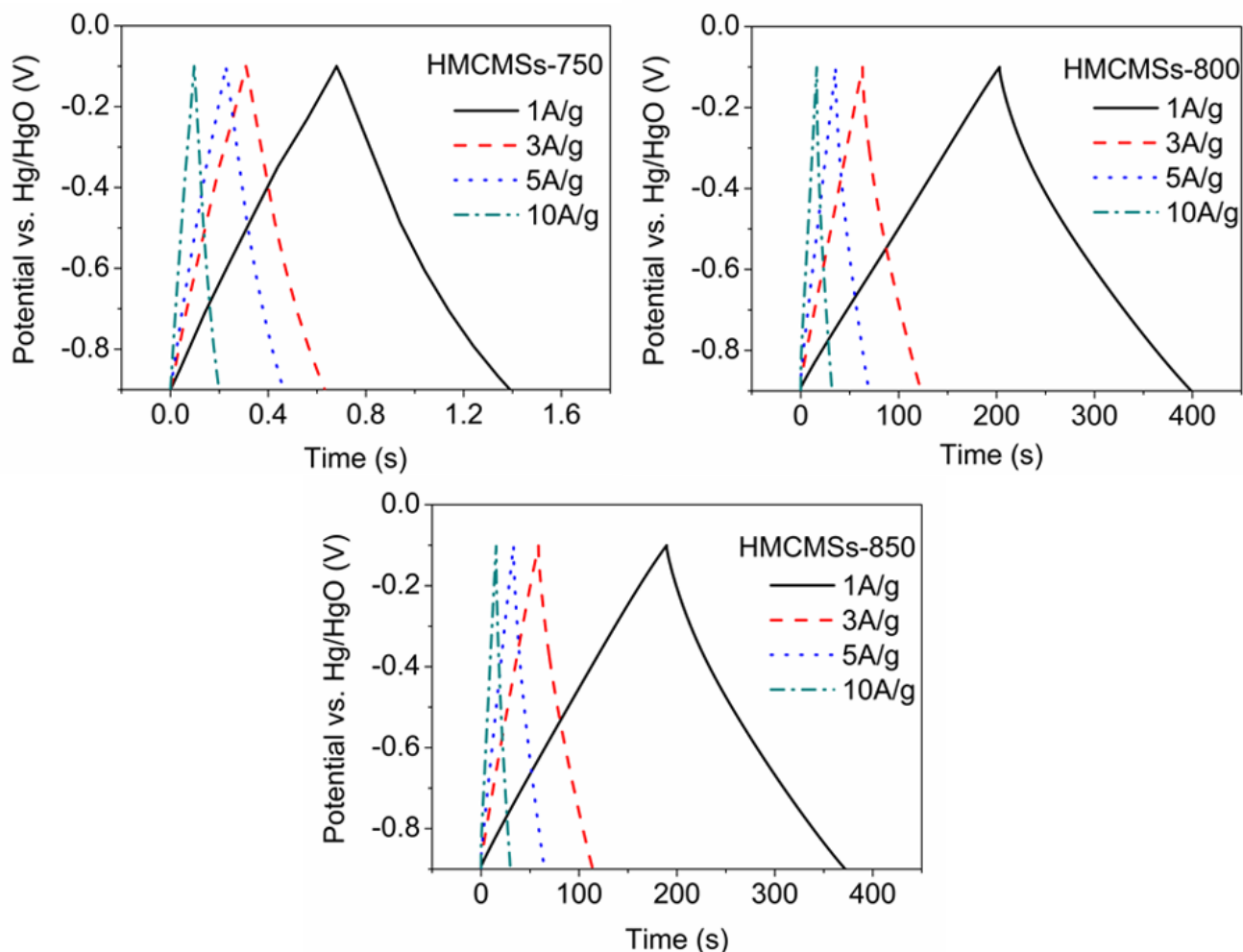


Figure 6. Galvanostatic charge-discharge splines of HMCMSs recorded at different ampere densities

4. CONCLUSION

A facile method to prepare HMCMSs has been presented here from a novel precursor PMSs. The highly cross-linked structure and high level of heteroatoms of PMSs play a key role to the formation of HMCMSs with large BET surface area and well-developed mesopore structure. HMCMSs with high heteroatoms doping (5.1–18.31 at%), and in particular, high specific surface area (1854–1956 m²/g) and uniform mesopore structure (~3 nm), exhibit the maximum specific capacitance of 274 F/g in 6 M KOH with the ampere density of 0.2 A/g. Additionally, the HMCMSs exhibit excellent electrochemical stability with 98.4% capacitive preservation even after 2000 cycles. The excellent supercapacitor performance profits by the large amount of heteroatoms, the high surface area and united mesopore structure that afford convenience of electrolyte ion transport. This work provides an effective strategy to prepare mesoporous carbon materials and used them as high performance supercapacitor electrode materials.

ACKNOWLEDGEMENTS

We gratefully acknowledge Natural Science Foundation of China (No. 21274092, 91441205), and Shanghai Science & Technology Committee (No. 10ZR1416100) for financial support.

References

1. A González, E Goikolea, JA Barrena and R Mysyk, *Renewable and Sustainable Energy Reviews*, 58 (2016) 1189.
2. A Rodriguez-Silva, O Movil-Cabrera, C Oliveira dos Anjos, J Staser, *Journal of the Electrochemical Society*, 163 (2016) B256.
3. Y Zheng, W Pann, D Zhengen, C Sun, *Journal of the Electrochemical Society*, 163 (2016) D230.
4. C Zhong, Y Deng, W Hu, J Qiao, L Zhang, *Chemical Society Reviews*, 41 (2012) 797.
5. F Béguin, V Presser, A Balducci, E Frackowiak, *Advanced Materials*, 26 (2014) 2219.
6. R Palm, H Kurig, T Romann, U Joost, R Kanarbik, R Väli, I Tallo, T Thomberg, A Jänes, E Lust, *Journal of the Electrochemical Society*, 164 (2017) A453.
7. Y. Rangom, X. Tang, L.F. Nazar, *ACS Nano*, 9 (2015) 7248.
8. J Liu, X Wang, Q Lu, R Yu, M Chen, S Cai, and X Wang, *Journal of the Electrochemical Society*, 163 (2016) A2991.
9. K Chen, X Huang, C Wan, H Liu, *Electrochimica Acta*, 222 (2016) 543.
10. Z Geng, H Wang, R Wang, P Zhang, J Lang, *Materials Letters*, 182 (2016) 1.
11. Yoon, SM Oh, CW Lee, HR Ji, *Journal of Electroanalytical Chemistry*, 650 (2011) 187.
12. L Qie, WM Chen, ZH Wang, QG Shao, X Li, *Advanced Materials*, 24 (2012) 2047.
13. W Si, J Zhou, S Zhang, S Li, W Xing, *Electrochimica Acta*, 107 (2013) 397.
14. K Chen, X Huang, C Wan, H Liu, *Materials Chemistry and Physics*, 164 (2015) 85.
15. W. Wei, R. Lu, S. Tang, X. Liu, *Journal of Materials Chemistry A*, 3 (2015) 4604.
16. J Liu, X Wang, Q Lu, R Yu, M Chen, S Cai, X Wang, *Journal of the Electrochemical Society*, 163 (2016) A2991.
17. SK Ramasahayam, Z Hicks, T Viswanathan, *Acs Sustainable Chemistry & Engineering*, 3 (2015) 21942.
18. E Roumeli, A Avgeropoulos, E Pavlidou, G Vourlias, T Kyratsi, *Rsc Advances*, 4 (2014) 45522.
19. S Yang, X Song, P Zhang, J Sun, L Gao, *Small*, 10 (2014) 2270.
20. M Klein, A Varvak, E Segal, B Markovsky, IN Pulidindi, *Green Chemistry*, 17 (2015) 2418.
21. H Xia, C Hong, B Li, B Zhao, Z Lin, *Advanced Functional Materials*, 25 (2015) 627.
22. M Li, C Liu, H Cao, H Zhao, Y Zhang, *Journal of Materials Chemistry A*, 2 (2014) 14844.
23. J Zhou, T Zhu, W Xing, Z Li, H Shen, *Electrochimica Acta*, 160 (2015) 152.
24. Z Fan, J Yan, T Wei, L Zhi, G Ning, *Advanced Functional Materials*, 21 (2011) 2366.
25. WY Tsai, PC Gao, B Daffos, PL Taberna, CR Perez, *Electrochemistry Communications*, 34 (2013) 109.
26. S Uppugalla, U Male, P Srinivasan, *Electrochimica Acta*, 146 (2014) 242.
27. B You, F Kang, P Yin, Q Zhang, *Carbon*, 103 (2016) 9.
28. S. Bose, T. Kuila, A.K. Mishra, R. Rajasekar, N.H. Kim, J.H. Lee, *Journal of Materials Chemistry*, 22 (2012) 767.
29. M Deraman, NSM Nor, NH Basri, BNM Dollah, S Soltaninejad, *Advanced Materials Research*, 1112 (2015) 231.
30. SJ Park, DW Kim, JH Lee, *Journal of Nanoscience & Nanotechnology*, 14 (2014) 9263.
31. J. Gamby, P. L. Taberna, P. Simon, J. F. Fauvarque, *J. Power Sources* 101 (2001) 109.
32. Ping Cheng, Ting Li, Hang Yu, Lei Zhi, *The Journal of Physical Chemistry C*, 120 (2016) 4.
33. Qian Cheng, Jie Tang, Norio Shinya, Luchang Qin, *Science and Technology of Advanced Materials*, 15 (2014) 14206.

34. Dacheng Zhang, Xiong Zhang, Yao Chen, Peng Yu, Changhui Wang, Yanwei Ma, *Journal of Power Sources*, 196 (2011) 5990.
35. Chao Peng, Xingbin Yan, Rutao Wang, Junwei Lang, Yujing Ou, Qunji Xue, *Electrochimica Acta*, 87 (2013) 401.

© 2017 The Authors. Published by ESG (www.electrochemsci.org). This article is an open access article distributed under the terms and conditions of the Creative Commons Attribution license (<http://creativecommons.org/licenses/by/4.0/>).